www.Cheshme.in

Journal of Constructional Steel Research 117 (2016) 24–34

Contents lists available at ScienceDirect

Journal of Constructional Steel Research

Cyclic behavior of seesaw energy dissipation system with steel slit dampers

Hiroshi Tagawa [a,*], Teruaki Yamanishi [a], Akira Takaki [a], Ricky W.K. Chan [b]

[a] Graduate School of Engineering, Hiroshima University, Japan
[b] School of Civil, Environmental and Chemical Engineering, RMIT University, Australia

ARTICLE INFO

Article history:
Received 1 April 2015
Received in revised form 23 September 2015
Accepted 25 September 2015
Available online xxxx

Keywords:
Passive control
Slit damper
Seesaw system
Energy dissipation
Seismic protection

ABSTRACT

This paper presents an investigation into the cyclic behavior of a passive vibration control system in which steel slit dampers are applied to a seesaw energy dissipation system. The fundamental concept of the seesaw system is the quasi-linear motion mechanism, which enables the bracing members to remain in tension during vibration. The lateral stiffness and strength formulae of the frame with this system are derived first. Six cyclic loading tests were conducted to reveal that the proposed system has a stable hysteretic property and a large energy dissipation capacity. For all specimens, the slit dampers yielded at early stages of the tests around a story rotation angle of 0.001 rad. This property is preferred for energy dissipation properties to reduce story drift in building structures under seismic loads. The important seesaw system characteristic of the bracing members remaining tensile was also observed. The tri-linear hysteretic model is introduced to model the cyclic behavior of the proposed damping system. A comparison of the hysteretic loops and the energy dissipation amount between the model and test results reveals the adaptability of the tri-linear model to the hysteretic behavior of the proposed system. The validity of the stiffness and strength prediction is also shown from the test results.

1. Introduction

During a severe earthquake, the significant amount of energy input to a structure can cause structural damage. For earthquake risk mitigation in structures, extensive studies of passive energy dissipation methods have been conducted [1]. Some of the input seismic energy can be diverted into energy dissipation devices installed within a structure. Among such devices, a steel damper dissipates seismic energy through the yield deformation of steel materials. Therefore, this is categorized as a so-called hysteretic damper [2]. For example, the buckling-restrained braces dissipate seismic energy through the axial yielding of steel core members [3–7]. The steel shear panels dissipate seismic energy through shear yielding [8]. In addition, the TADAS [9], the U-shaped dampers [10,11], slit dampers [12], and pipe dampers [13] dissipate seismic energy through flexural yielding. Slit dampers are used, for example, at brace members [14] and at beam-to-column connections [15,16].

A previous study [11] investigated an energy dissipation system based on a quasi-linear motion mechanism realized by three link members called a Chebyshev linkage, as presented in Fig. 1(a–c). Multiple dampers placed at both ends of a rotatable member dissipate energy by compression and tension deformation, as presented in Fig. 1(b). This energy dissipation system is designated as a seesaw system because the rotatable member moves similarly to that of a seesaw [17]. One benefit of this system is that it enables the usage of steel rods or cables as bracing because the bracing members with pre-tension retain their tension during vibration. Various kinds of dampers are available for this system. First, U-shaped steel dampers were adopted and investigated through static cyclic loading tests [11]. In subsequent studies, velocity-dependent dampers such as viscoelastic dampers [17] and fluid viscous dampers [18] were also adopted for the seismic response analyses of building frames. A recent study [19] examined friction dampers for a case in which a seesaw member was installed vertically, as presented in Fig. 1(d).

Some cyclic loading tests conducted for the seesaw system with U-dampers showed the stable hysteresis loops and large ductility of the damping system [11]. The results showed, however, that the lateral stiffness of the damping system was rather low, which resulted from the low bending stiffness of the U-dampers. For that reason, late damper yielding occurred when the story rotation angle reached about 0.005 rad. This property is not preferred from the perspective of energy dissipation properties to reduce the story drift of structures under seismic loads.

This study investigates the application of steel slit dampers to the seesaw system for increasing the damper stiffness and improving the energy dissipation property. In this paper, the lateral story stiffness and strength formulae are first derived for the seesaw system with slit dampers. The energy dissipation property of the proposed system is revealed from the results of six cyclic loading tests. Finally, a tri-linear hysteretic model is introduced to represent the cyclic behavior

* Corresponding author.
E-mail address: htagawa@hiroshima-u.ac.jp (H. Tagawa).

http://dx.doi.org/10.1016/j.jcsr.2015.09.014
0143-974X/

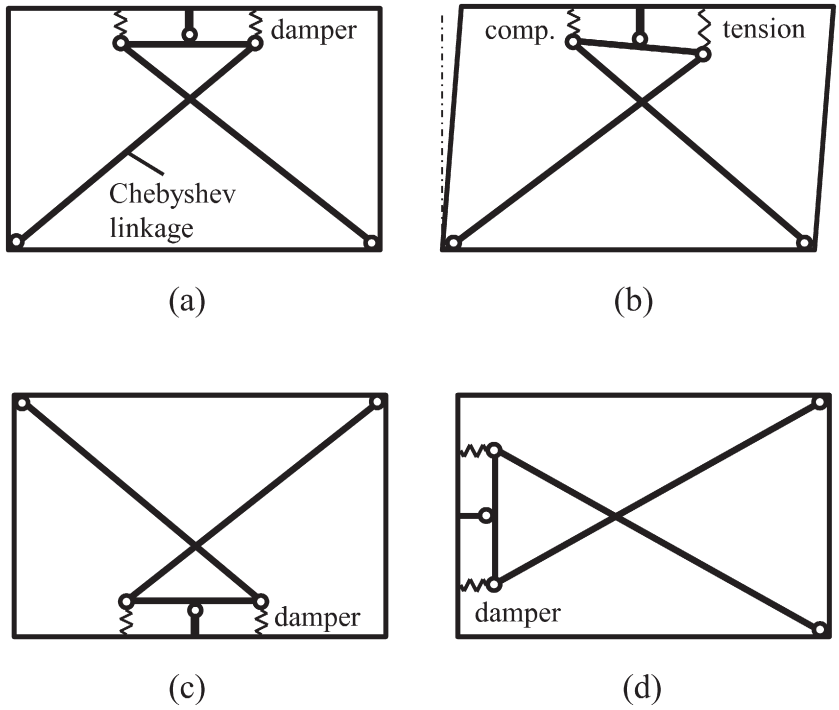

Fig. 1. Concept of seesaw energy dissipation system: (a) initial configuration, (b) deformed configuration, (c) bottom installation type, (d) vertical installation type.

of the proposed system in a simple manner. The validity of the stiffness and strength prediction and the adaptability of the hysteretic model are examined by comparing the cyclic loading test results.

2. Lateral stiffness and strength evaluation

2.1. Outline of seesaw system with steel slit dampers

Fig. 2 presents the seesaw energy dissipation system with steel slit dampers. Multiple slit dampers are installed under the seesaw member. When a lateral force F acts on the frame, the brace's tensile force acts on the seesaw member edge. The frame lateral displacement is denoted by δ as shown in Fig. 2(b). The seesaw member rotation around the pin forces the slit dampers to deform as presented in Fig. 2(b). The slit dampers exhibit plastic deformation and dissipate energy. By providing pre-tension force to the bracing members, it is expected that the tensile axial force remains in both bracing members during the frame deformation [11].

2.2. Slit damper stiffness and strength

The shape and dimensions of a steel slit damper are presented in Fig. 3. It is assumed that one side of the damper is fixed and the other side is roller supported. The relationship between the shear force f_D and displacement u_D is expressed as.

$$f_D = k_D u_D. \tag{1}$$

In Eq. (1), k_D denoting the damper stiffness is obtained by.

$$k_D = 1/\left(\frac{h'}{3Gtb} + \frac{h'^3}{3Etb^3}\right), \tag{2}$$

where G signifies the shear modulus, E represents the Young's modulus, and t denotes the steel plate thickness. Also, h' is the equivalent strut length [14,15] as presented in Fig. 4.

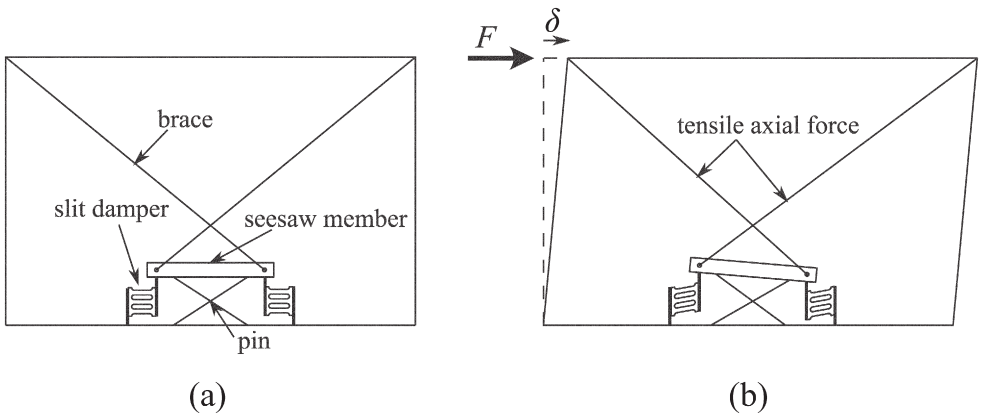

Fig. 2. Seesaw system with steel slit dampers: (a) initial configuration and (b) deformed configuration.

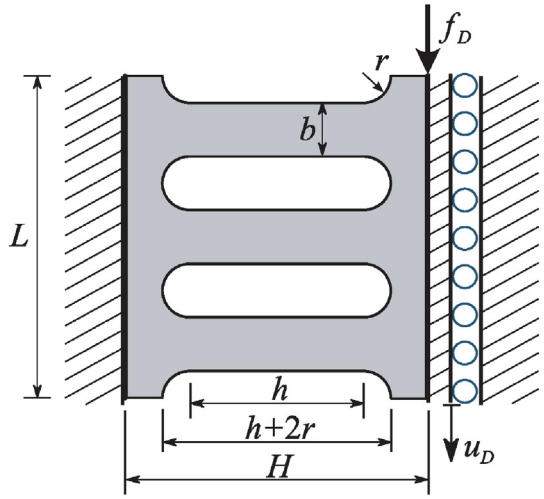

Fig. 3. Shape and dimensions of slit damper.

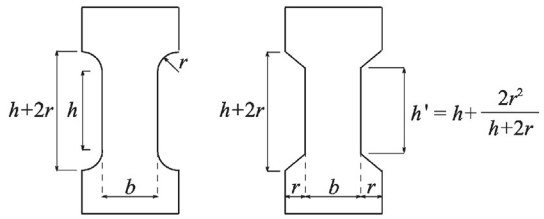

Fig. 4. Equivalent strut length.

The plastic failure load of the damper is expressed as

$$f_D^P = \frac{6M_P}{h'} = \frac{3\sigma_y b^2 t}{2h'}, \tag{3}$$

where M_P signifies the full-plastic moment of the damper plate at the parallel portion of the strut, and σ_y represents the yield stress of the steel damper material.

2.3. Lateral system stiffness and strength

Fig. 5 presents a simplification of the analytical model. The displacements of the left and right dampers can be assumed as equal if the seesaw member is sufficiently stiff. Furthermore, the brace's axial force can be assumed to maintain tension by introducing a proper amount of pre-tension force. Under this assumption, the system can be modeled using the simple model shown in Fig. 5(b). This simple model is obtained by modifying the damper part of the simple model using fluid viscous dampers [18]. In Fig. 5(b), α represents the horizontal angle of the brace, and β denotes the horizontal angle of the line AB. The relationship between the brace axial force F_B and its deformation δ_B is as follows:

$$F_B = 2k_B\delta_B. \tag{4}$$

Therein, k_B denotes the rod stiffness. The relationship between the damper force F_D and its deformation δ_D is.

$$F_D = 2k_D\delta_D, \tag{5}$$

where k_D denotes the damper stiffness expressed with Eq. (2). The damper deformation δ_D corresponds to the displacement u_D as presented in Fig. 3. Therefore, the damper force F_D is twice that of the shear force f_D.

According to Fig. 5(b), the relationship between the lateral force F and the brace axial force F_B is expressed as.

$$F = F_B\cos\alpha. \tag{6}$$

Considering the moment equilibrium about the seesaw pin (point A), the following relationship is obtained:

$$F_B = \frac{w + s/2}{e} F_D. \tag{7}$$

In that equation, w denotes the lateral distance between points A and B, s represents the lateral distance between point B and the

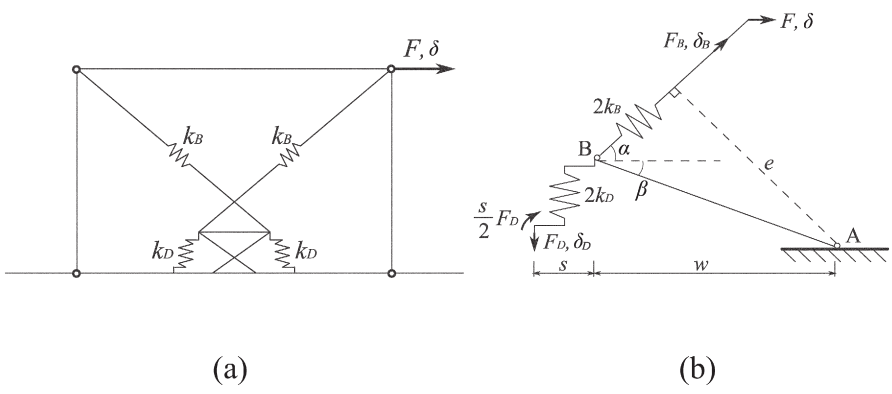

Fig. 5. Simplification of analytical model: (a) exact model and (b) simple model.

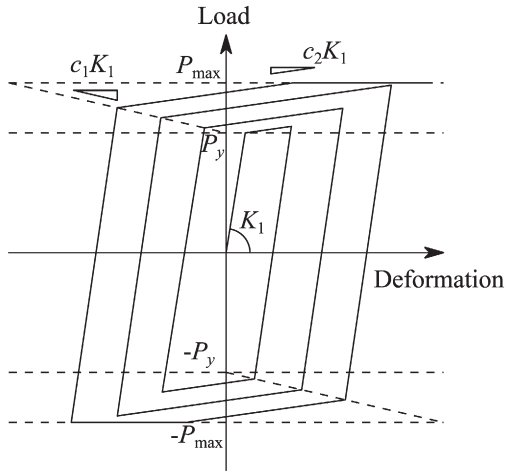

Fig. 6. Tri-linear hysteretic model.

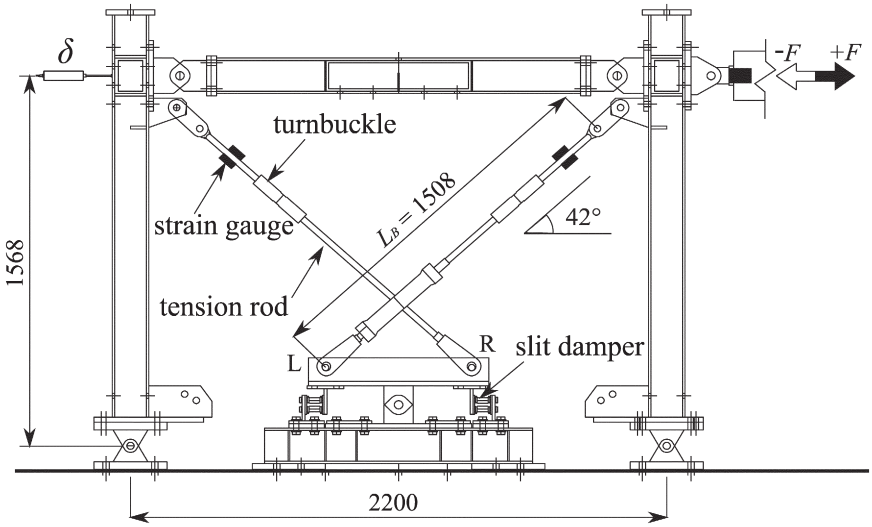

Fig. 7. Test specimen with loading and measuring system.

damper end, and e is the perpendicular distance between point A and the brace, as presented in Fig. 5(b).

According to an earlier study [18], the relationship among the displacements δ, δ_D, and δ_B is expressed as:

$$\delta_D = f_R\delta - \frac{f_R}{\cos\alpha}\delta_B, \tag{8}$$

$$f_R = \frac{\cos\alpha\cos\beta}{\sin(\alpha+\beta)}, \tag{9}$$

Where f_R represents the magnification factor of the seesaw system when the brace is assumed to be rigid. Eq. (8) is valid for the case in which the seesaw member is sufficiently stiff. For the case in which the seesaw member is not stiff, an earlier study [11] provided stiffness formulae considering the seesaw member deformation.

From Eqs. (4)–(9), the lateral system stiffness k can be obtained as follows:

$$k = \frac{F}{\delta} = \frac{f_R\cos\alpha}{\frac{1}{2k_D}\frac{e}{w+s/2} + \frac{1}{2k_B}\frac{f_R}{\cos\alpha}}. \tag{10}$$

The lateral system strength F_u is obtained from Eqs. (3), (6), and (7) as shown below.

$$F_u = 2f_D^p\frac{w+s/2}{e}\cos\alpha. \tag{11}$$

The plus sign in Eq. (11) changes to a minus sign for the case in which the dampers are placed at the inner position, as presented in Section 3.3. Therefore, the damper placement influences the lateral strength to a great degree.

Table 1
Damper dimensions (units: mm).

	L-9.0	S-9.0	S-4.5
L	72	72	72
b	12	12	12
H	141	66	66
h	113	38	38
r	6	6	6
t	9	9	4.5

2.4. Hysteretic model of cyclic behavior

In the design process for structures with energy dissipation systems, seismic response analyses are commonly conducted to examine the damping system performance. For that purpose, a hysteretic model of the damping system is effective at decreasing the calculation time and cost. Ref. [20], for example, provides a database for hysteretic models of the cyclic behavior of steel dampers such as shear panels and buckling restrained braces. This study applies a tri-linear model [20], as shown in Fig. 6, to represent the relationship between the lateral force F and the displacement δ (story rotation angle R) in the cyclic behavior of the proposed energy dissipation system. In this hysteretic model, the yield strength increases linearly with the vibration amplitude. The five parameters of K_1, P_y, P_{max}, c_1, and c_2 are used, where K_1 denotes the elastic stiffness, P_y represents the initial yield strength, P_{max} represents the maximum strength, c_1 denotes the increase ratio of the yield strength with respect to the amplitude, and c_2 is the second stiffness ratio. The values of K_1 and P_y are obtainable from Eqs. (10) and (11), respectively. P_{max}, c_1, and c_2 are determined from the test results, as presented in the following chapter.

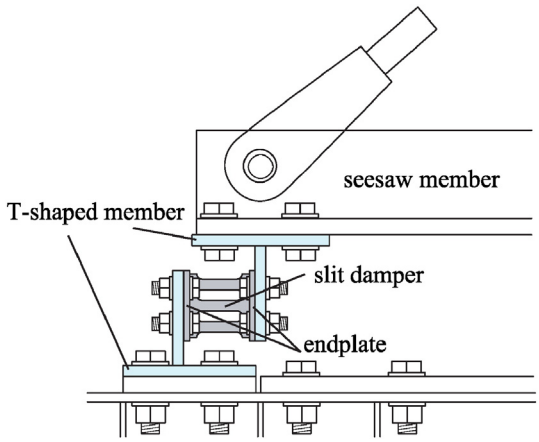

Fig. 8. Details of damper attachment.

Table 2
Material properties.

	Yield stress (N/mm^2)	Ultimate stress (N/mm^2)	Elongation (%)
L-9.0(-c)	314	446	42
S-9.0(-i)	317	444	42
S-4.5(-i)	310	440	39

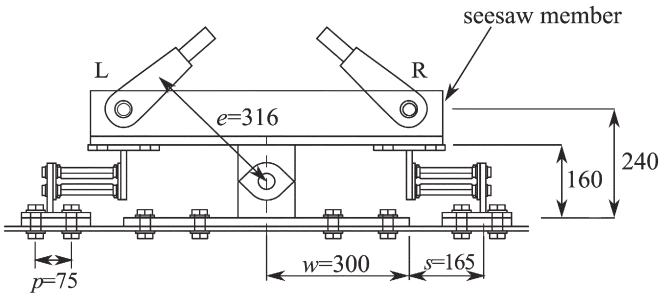

(a) Specimens L-9.0 and L-9.0-c

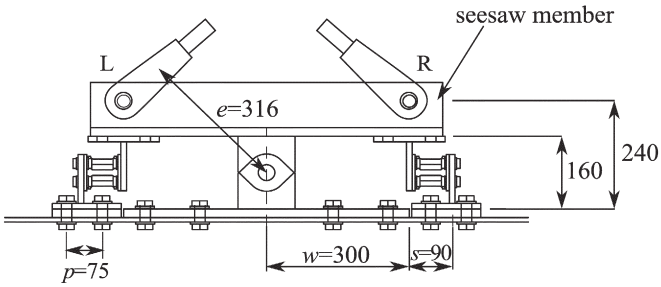

(b) Specimens S-4.5 and S-9.0

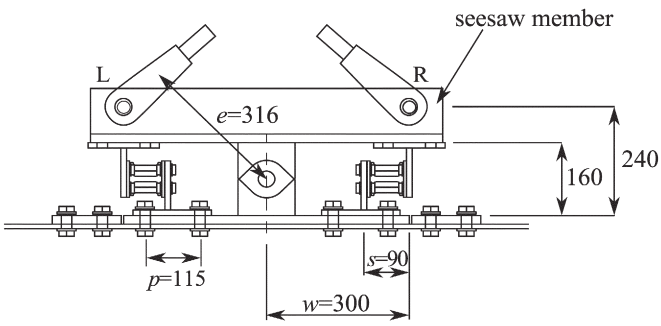

(c) Specimens S-4.5-i and S-9.0-i

Fig. 9. Damper shapes and placements.

Table 3
List of test specimens.

Test specimen	Strut length	Damper thickness	Damper position	Loading amplitude
L-9.0	Long	9 mm	Outer	Increasing
L-9.0-c	Long	9 mm	Outer	Constant
S-9.0	Short	9 mm	Outer	Increasing
S-9.0-i	Short	9 mm	Inner	Increasing
S-4.5	Short	4.5 mm	Outer	Increasing
S-4.5-i	Short	4.5 mm	Inner	Increasing

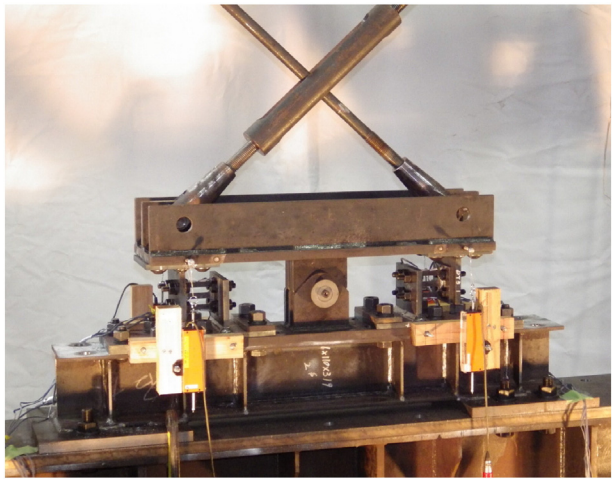

Fig. 10. Seesaw member with slit dampers in specimen S-4.5-i.

3. Cyclic loading tests

3.1. Test specimens

An overview of the test specimen is presented in Fig. 7. The column and beam members of H–150 × 150 × 7 × 10 (steel grade: SN400B) are connected by pin joints. The columns are also fixed by pin supports at

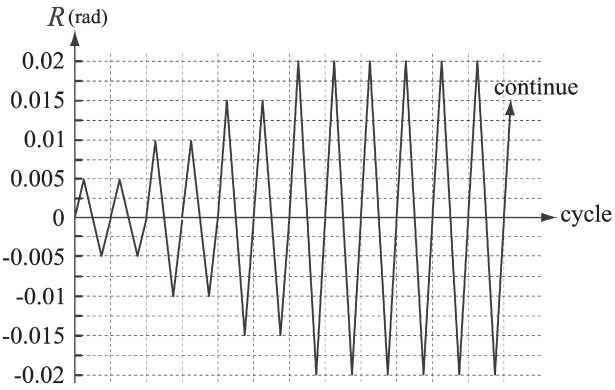

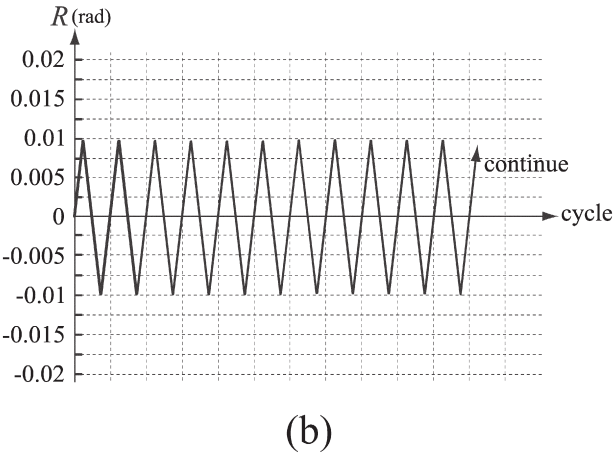

Fig. 11. Loading history: (a) increasing amplitude and (b) constant amplitude.

the bottom. Consequently, the lateral stiffness and strength of the test specimens are dependent only on the damper system including the bracing. It is noteworthy that this damper system is also available together with the moment frame. Out-of-plane movement of the frame is prevented at the column tops. The bracing members are 25-mm-diameter tension rods (steel grade: SS400). A cross-turnbuckle component is used for the intersection part of the bracing members to avoid their contact [11]. The 19-mm-thick steel plates used as seesaw members are stiffened with rib plates to suppress their deformation. Before damper placement, a brace pre-tension of 40 kN corresponding to 400 μ strain is introduced using the turnbuckles. The brace's axial force is monitored during the tests using strain gauges mounted on both sides near the upper edge.

After the steel plates are manufactured as shown in Fig. 3 and Table 1, end plates are welded at both sides. The T-shaped members are used for the damper attachment as presented in Fig. 8, where high-strength bolts are used for the connection. Table 2 presents the damper material properties obtained using the tensile coupon tests. Fig. 9 presents the details of the seesaw member with different slit damper shapes. The test parameters include the plate thickness (4.5 mm and 9 mm), the strut length (38 mm (short) and 113 mm (long)), and the damper placement (inner and outer position). Table 3

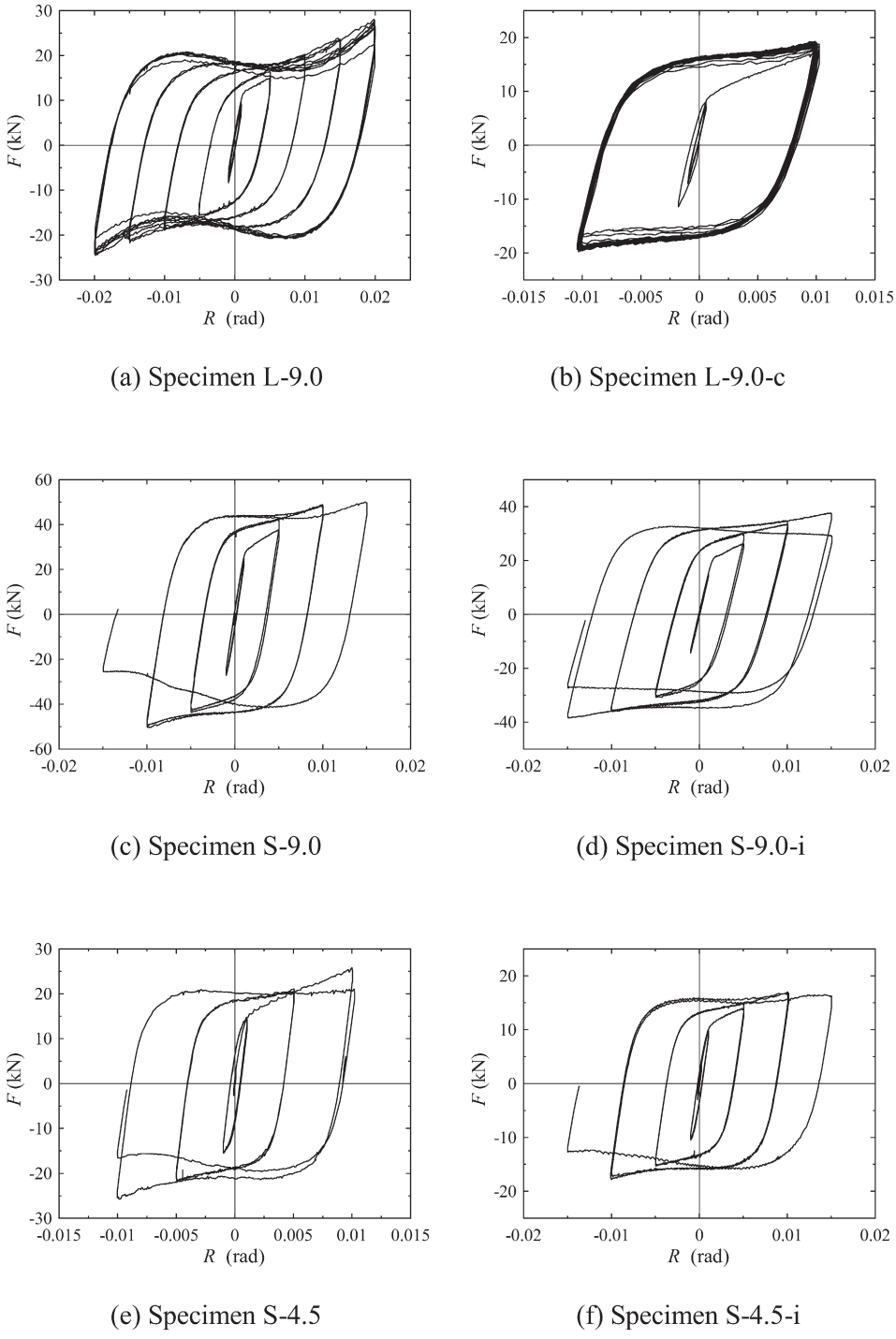

Fig. 12. Lateral load and story rotation angle relationship.

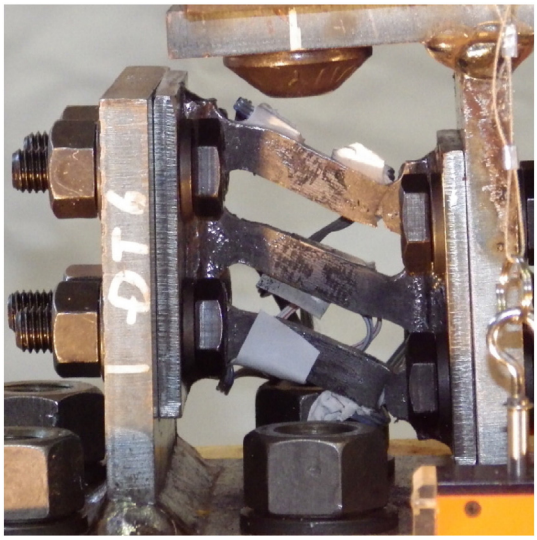

Fig. 13. Damper deformation in specimen S-9.0 at $R = -0.015$ rad.

presents six test specimens. In Fig. 9, p denotes the distance between the bolts used for the lower T-shaped member attachment. The distance of $p = 115$ mm for specimens S-4.5-i and S-9.0-i is rather long to avoid vertical stiffeners, as shown in Figs. 7 and 8. A photograph of the seesaw member in specimen S-4.5-i is presented in Fig. 10.

3.2. Loading programs

Fig. 7 shows that a lateral load F is applied at the right beam-to-column connection under control of the lateral displacement δ measured at the left beam-to-column connection. Fig. 11 shows the loading program for the two types adopted in this study. For the loading condition of gradually increasing amplitude (Fig. 11(a)), the lateral load F was varied to obtain an increasing story rotation angle R ($=\delta/1568$) equal to 0.001, 0.005, 0.01, 0.015, and 0.02 rad. For each rotation angle, two full cycles of loading were performed. Then, under a constant amplitude of $R = 0.02$ rad, the cyclic loading continued until strength deterioration occurred. For specimen L-9.0-c only, a constant amplitude (Fig. 11(b)) was adopted from the beginning of the loading, in which the lateral load F was applied cyclically under a constant amplitude of $R = 0.01$ rad.

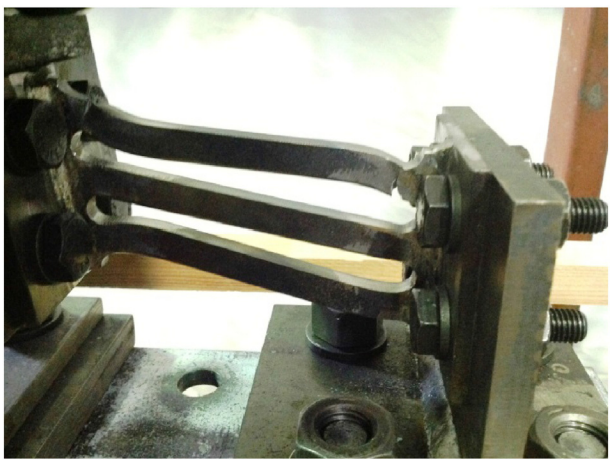

Fig. 14. Damper failure in specimen L-9.0-c at the final stage.

Table 4
Lateral stiffness and strength.

	Lateral stiffness in kN/mm			Lateral strength in kN		
	k_{eval}	k_{test}	k_{eval}/k_{test}	${F_u}^{eval}$	${F_u}^{test}$	${F_u}^{eval}/{F_u}^{test}$
L-9.0	5.4	5.3	1.02	10.0	11.8	0.85
S-9.0	13.8	13.7	1.01	25.8	28.0	0.92
S-9.0-i	13.2	9.0	1.47	19.1	21.5	0.91
S-4.5	12.6	12.6	1.00	12.6	14.0	0.96
S-4.5-i	11.8	7.5	1.57	9.3	10.9	0.91

3.3. Test results

3.3.1. Load and story drift relationship

Fig. 12 presents the lateral load F and story rotation angle R relationships. All of the specimens exhibited stable hysteretic loops. The dampers yielded at early stages of the tests around $R = 0.001$ rad. This result demonstrates that the proposed seesaw system with slit dampers has good energy dissipation characteristics. For specimens S-9.0 and S-4.5, lateral strength deterioration occurred, and therefore, the loadings were terminated before $R = 0.02$ rad. In these specimens, the slit damper deformation per unit story rotation angle was rather large, which leads to large damper deformation even at $R = 0.015$ rad, as shown in Fig. 13. By contrast, specimen L-9.0 (having a longer strut length) exhibited an improvement in the deformation capacity, where for $R = 0.02$ rad, seven loading cycles were attained before lateral strength deterioration was observed. In this paper, the strength deterioration occurrence is defined as the point at which a 10% strength reduction from the maximum strength is observed.

Specimen L-9.0-c was tested to reveal the cyclic fatigue property. Under a constant amplitude of $R = 0.01$ rad, strength deterioration occurred after 27.5 loading cycles. This result indicates that the proposed passive damping system with slit dampers has a high energy dissipation capacity. Fig. 14 presents a photograph of the slit damper in specimen L-9.0-c at the final stage of loading.

The cumulative plastic deformation ratio η is defined as follows:

$$\eta = \frac{\left|{}_{cum}\delta_p^+\right| + \left|{}_{cum}\delta_p^-\right|}{\delta_y}, \tag{12}$$

where ${}_{cum}\delta_p^+$ and ${}_{cum}\delta_p^-$ represent the cumulative plastic displacement in the positive and negative loading directions, respectively. Those values can be obtained by splitting the load and displacement curve [14]. Here, δ_y represents the lateral yield displacement of the frame. An η value of 592 was recorded for specimen L-9.0-c until strength deterioration occurred. A value of 472 was recorded for specimen L-9.0, in which the cyclic loads at a constant amplitude of $R = 0.02$ rad acted for the final seven cycles. It was found that the magnitude of the loading amplitude influenced the plastic deformation capacity.

Table 4 presents the lateral stiffness k_{test} and strength ${F_u}^{test}$ measured in the tests. The lateral strength was obtained as the lateral load at which the lateral stiffness reached one-third of the initial stiffness. The predicted lateral stiffness k_{eval} obtained with Eq. (10) and the strength ${F_u}^{eval}$ obtained with Eq. (11) are shown in Table 4, where the ratios of the prediction to test values are also presented. For the case in which the dampers are placed at the inner position, as shown in Fig. 9(c), a minus sign should be used instead of the plus sign just before $s/2$ in Eqs. (7), (10), and (11).

The ratio values reveal good prediction accuracies except for the lateral stiffness of specimens S-9.0-i and S-4.5-i, where the predicted stiffness was higher than the test value. Regarding the reason for this, the following conjecture was made. As described in Section 3.1 with Fig. 9, the bolt distance of $p = 115$ mm was rather long for these specimens. That possibly leads to a deformation of the T-shaped members in addition to the dampers and thereby induces a reduction in the lateral

stiffness of the frame. Furthermore, the seesaw member rotation for the specimens with an inner damper placement has the effect of reducing the damper stiffness. This effect is not significant rather than the flexibility of the base plate with $p = 115$ mm as stated above but explained in detail in Appendix A.

Comparing specimens S-4.5 (S-9.0) and S-4.5-i (S-9.0-i), the lateral strengths of specimens S-4.5 and S-9.0, in which the dampers were placed at the outer positions, were larger than those of S-4.5-i and S-9.0-i. This difference in lateral strength is explainable with Eq. (11), in which the plus sign changes to a minus sign for specimens S-4.5-i and S-9.0-i.

3.3.2. Brace behaviors

Fig. 15 presents the lateral load and brace axial force relationship. The letters R and L in the figure denote the brace members connected to the right and left side dampers, respectively, as shown in Figs. 7 and 9. Under cyclic loading, the brace's axial forces increase and decrease cyclically around the pre-tension force of 40 kN. For all specimens, the results show that the brace axial force remains tensile during the tests, which means that the brace's axial deformation is extremely small. When the story rotation angle R is 0.01 rad, the lateral displacement of the frame is about 15 mm. Considering that the brace inclination angle is 42°, the brace member's axial deformation at $R = 0.01$ rad

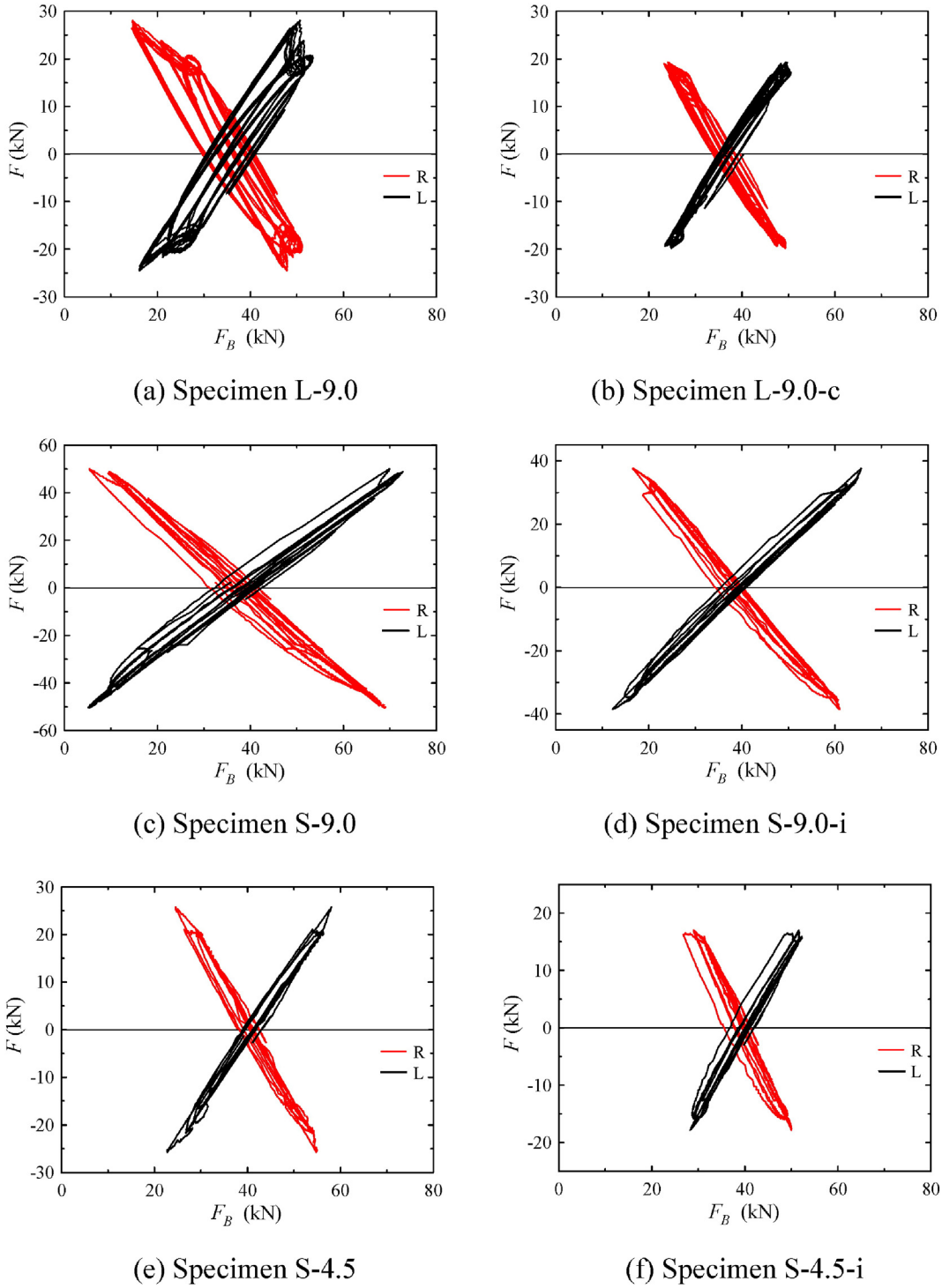

Fig. 15. Lateral load and brace axial force relationship.

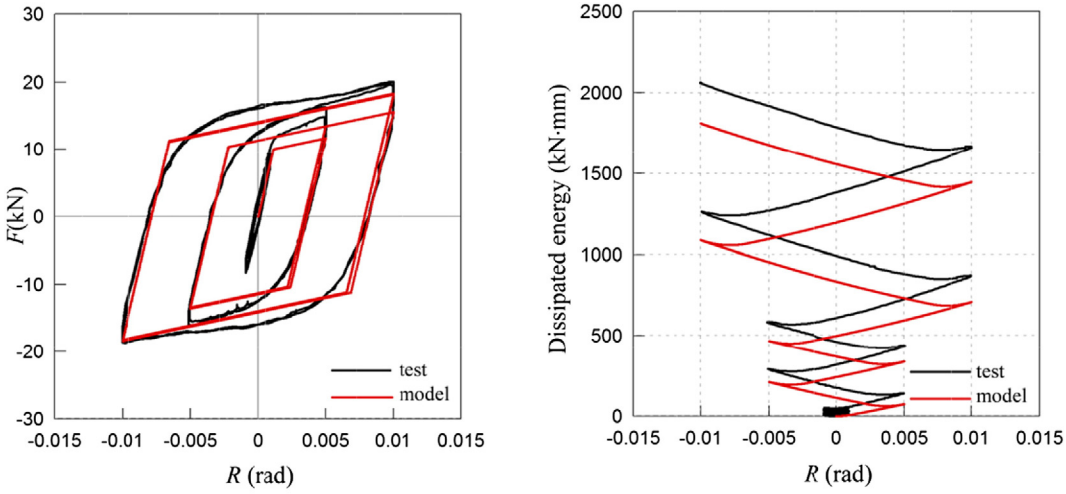

(a) Specimen L-9.0

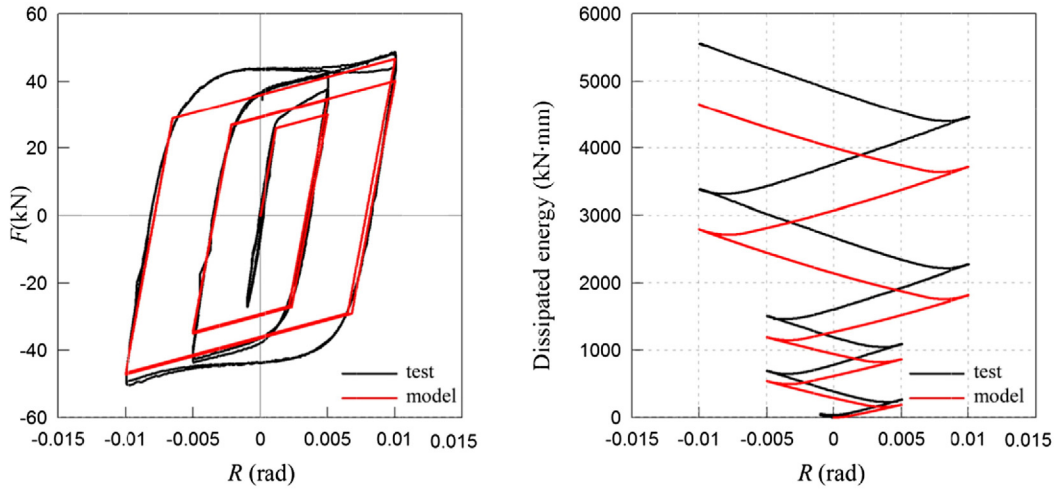

(b) Specimen S-9.0

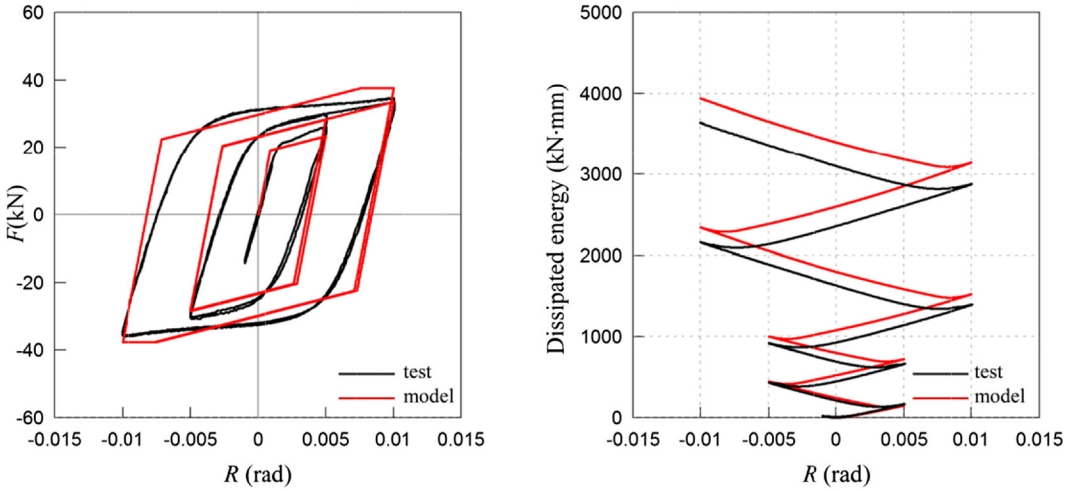

(c) Specimen S-9.0-i

Fig. 16. Comparison of hysteretic model with test results.

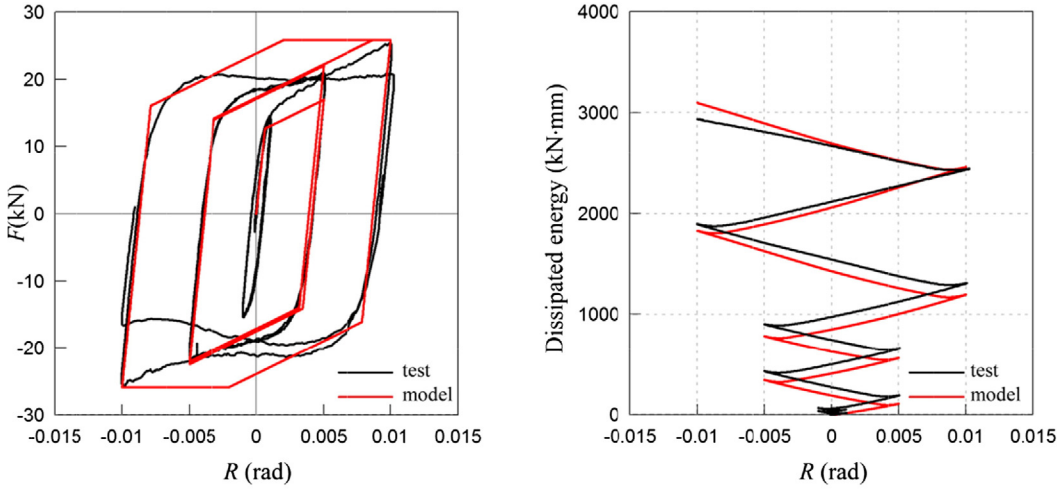

(d) Specimen S-4.5

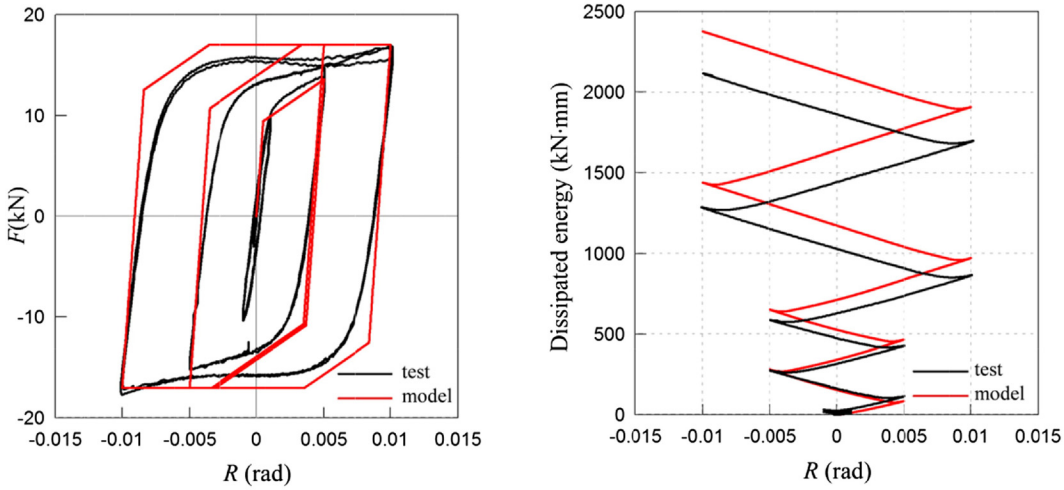

(e) Specimen S-4.5-i

Fig. 16 (*continued*).

might exceed 10 mm if the seesaw member does not rotate. The brace's axial deformation of 10 mm is much larger than the yield deformation, which indicates that the seesaw member rotation is fundamentally important for the seesaw system. Furthermore, the variations in the absolute values of the brace's axial force are almost identical in both braces, as presented in Fig. 15. These are also important characteristics attributable to the quasi-linear motion mechanism [11,21], as presented in Fig. 1.

Table 5
Comparison of total dissipated energy.

	E_{model} (kN mm)	E_{test} (kN mm)	E_{model}/E_{test}
L-9.0	1811	2066	0.88
S-9.0	4651	5528	0.84
S-9.0-i	3943	3628	1.09
S-4.5	3096	2930	1.06
S-4.5-i	2377	2105	1.13

3.3.3. Adaptability of tri-linear hysteretic model for cyclic behavior

Fig. 16 compares the tri-linear model and test results. The left panels show the lateral load and story rotation angle relation. The right panels show the energy dissipation and the story rotation angle relationship. For the determination of the tri-linear model, the test results up to $R = 0.01$ rad were used. The reasons for this limitation were as follows: (i) for specimen L-9.0, the hysteretic loop shape as shown in Fig. 12(a) becomes complex beyond $R = 0.01$ rad because of the slit damper geometry; (ii) for specimen S-4.5, strength deterioration occurred at $R = 0.01$ rad; and (iii) the story rotation angle of 0.01 rad is often used as the target maximum value for building frame designs with dampers.

As stated in Section 2.4, the elastic stiffness K_1 and the initial yield strength P_y are obtained by Eqs. (10) and (11) for the tri-linear model shown in Fig. 6. The values of k_{eval} and F_u^{eval} presented in Table 4 were used for determining the values of K_1 and P_y, respectively. The values $c_1 = 0.02$ and $c_2 = 0.05$ were adopted for all of the specimens. The adaptability of the model was first examined with the hysteretic loop shapes, i.e., the left panels of Fig. 16. Although a slight difference is apparent, the hysteretic model agrees well with the test results overall.

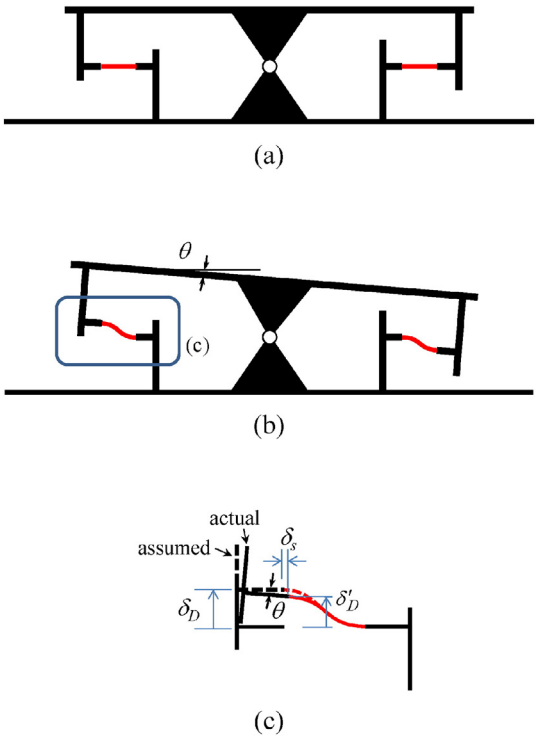

Fig. 17. Actual damper deformation for inner damper placement: (a) initial configuration, (b) deformed configuration, (c) enlarged view of left damper.

The adaptability of the model was examined with the energy dissipation [9,14], i.e., the right panels of Fig. 16. Table 5 presents a comparison of the total dissipated energy of the model E_{model} with that of the test E_{test}. Although the ratio of E_{model} to E_{test} fluctuates from 0.84 to 1.13, it can be stated that the tri-linear model possesses sufficient accuracy for practical use.

4. Conclusion

This paper presented a passive vibration control system with steel slit dampers. The application of the slit damper to a seesaw energy dissipation system was proposed. The lateral stiffness and strength formulae for the damping system were derived first. Six cyclic loading tests revealed that the proposed system had a stable hysteretic property and a large energy dissipation capacity. For all specimens, the dampers yielded at the early stages of the tests around a story rotation angle of 0.001 rad, which indicates that this study overcame the low stiffness problem observed in the previous study using U-shaped steel dampers. Furthermore, the damping performance can be controlled easily by the plate thickness, the strut length, and the steel slit damper placement.

The test results revealed the validity of the stiffness and strength prediction. The important characteristic that the bracing members remain in tension during the tests was also revealed. The tri-linear hysteretic model was introduced to model the cyclic behavior of the proposed damping system. Comparison of the hysteretic loops and the energy dissipation between the model and test results revealed the adaptability of the tri-linear model to the hysteretic behavior of the proposed system.

Appendix A. Stiffness reduction for specimens with inner damper placement.

Fig. 17 illustrates the damper deformation for the case with the inner damper placement configuration. For simplicity, the struts of each slit damper are represented by a red beam. The other parts are assumed to be rigid. Fig. 17(b) and (c) shows the deformed configuration when the seesaw member rotates by θ. As described in Section 2.2 with Fig. 3, the damper stiffness k_D is obtained under the assumption that one side of the damper displaces vertically. In the actual deformation, however, it displaces diagonally with a rotation angle θ as shown in Fig. 17(c). Because of this, the vertical displacement of the strut end decreases from δ_D to δ_D'. Furthermore, the strut end rotates by θ and displaces laterally by δ_s. These differences between the assumed and actual deformations possibly induce the overestimation of the damper stiffness.

References

[1] G.W. Housner, L.A. Bergman, T.K. Caughey, A.G. Chassiakos, R.O. Claus, S.F. Masri, et al., Structural control: past, present and future, J. Eng. Mech. ASCE 123 (9) (1997) 897–971.
[2] M. Nakashima, K. Saburi, B. Tsuji, Energy input and dissipation behavior of structures with hysteretic dampers, Earthq. Eng. Struct. Dyn. 25 (1996) 483–496.
[3] R. Sabelli, S. Mahin, C. Chang, Seismic demands on steel braced frame buildings with buckling-restrained braces, Eng. Struct. 25 (2003) 655–666.
[4] C.J. Black, N. Makris, I.D. Aiken, Component testing, seismic evaluation and characterization of buckling-restrained braces, J. Struct. Eng. ASCE 130 (6) (2004) 880–894.
[5] Q. Xie, State of the art of buckling-restrained braces in Asia, J. Constr. Steel Res. 61 (2005) 727–748.
[6] M. Iwata, M. Murai, Buckling-restrained brace using steel mortar planks: performance evaluation as a hysteretic damper, Earthq. Eng. Struct. Dyn. 35 (14) (2006) 180726.
[7] L.A. Fahnestock, J.M. Ricles, R. Sause, Experimental evaluation of a large-scale buckling-restrained braced frame, J. Struct. Eng. ASCE 133 (9) (2007) 1205–1214.
[8] R.W.K. Chan, F. Albermani, M.S. Williams, Evaluation of yielding shear panel device for passive energy dissipation, J. Constr. Steel Res. 65 (2009) 260–268.
[9] K. Tsai, H. Chen, C. Hong, Y. Su, Design of steel triangular plate energy absorbers for seismic-resistant construction, Earthquake Spectra 9 (3) (1993) 505–528.
[10] Y. Koetaka, P. Chusilp, Z. Zhang, M. Ando, K. Suita, K. Inoue, et al., Mechanical property of beam-to-column moment connection with hysteretic dampers for column weak axis, Eng. Struct. 27 (2005) 109–117.
[11] H. Tagawa, J. Gao, Evaluation of vibration control system with U-dampers based on quasi-linear motion mechanism, J. Constr. Steel Res. 70 (2012) 213–225.
[12] R.W.K. Chan, F. Albermani, Experimental study of steel slit damper for passive energy dissipation, Eng. Struct. 30 (2008) 1058–1066.
[13] S. Maleki, S. Mahjoubi, Dual-pipe damper, J. Constr. Steel Res. 85 (2013) 81–91.
[14] A. Benavent-Climent, A brace-type seismic damper based on yielding the walls of hollow structural sections, Eng. Struct. 32 (2010) 1113–1122.
[15] S.H. Oh, Y.J. Kim, H.S. Ryu, Seismic performance of steel structure with slit dampers, Eng. Struct. 31 (2009) 1997–2008.
[16] H. Saffari, A.A. Hedayat, N.M. Poorsadeghi, Post-Northridge connections with slit dampers to enhance strength and ductility, J. Constr. Steel Res. 80 (2013) 138–152.
[17] J.D. Kang, H. Tagawa, Seismic response of steel structures with seesaw systems using viscoelastic dampers, Earthq. Eng. Struct. Dyn. 42 (5) (2013) 779–794.
[18] J.D. Kang, H. Tagawa, Seismic performance of steel structures with seesaw energy dissipation system using fluid viscous dampers, Eng. Struct. 56 (2013) 431–442.
[19] R. Okada, H. Tagawa, T. Yamanishi, Cyclic performance characteristics of seesaw vibration control system of vertical installation type, Proceedings of Annual Research Meeting Chugoku Chapter, 38, Architectural Institute of Japan 2015, pp. 161–164 (in Japanese).
[20] JSSI, Design and Construction Manual for Passively Controlled Buildings, Second ed. Japan Society of Seismic Isolation, 2005 (in Japanese).
[21] H. Tagawa, J. Gao, Vibration control system with U-shaped steel dampers based on quasi-linear motion mechanism, Journal of Structural and Construction Engineering, 648, Architectural Institute of Japan 2010, pp. 443–451 (in Japanese).